https://doi.org/10.5194/egusphere-2022-83
Preprint. Discussion started: 22 June 2022

Building a Filter-Wheel Apparatus to Generate Spectroscopic Information from Cathodoluminescence Images Obtained in a Scanning Electron Microscope: Applications in Zircon Geochronology

Kristin Rabosky[1], Colin Inglefield[1], Elizabeth Balgord[2], Sarah Stamps[1], Chloe Jones[1], Martin Totland[1], Brycen Lee[1], Jeremy Mathews[1]

[1]Department of Physics and Astronomy, Weber State University, Ogden, UT, 84408, USA
[2]Department of Earth and Environmental Sciences, Weber State University, Ogden, UT, 84408, USA

Correspondence to: Kristin Rabosky (kristinrabosky@weber.edu) or Elizabeth Balgord (elizabethbalgord@weber.edu)

Abstract. We present a simple inexpensive design for a filter wheel to modify a broadband cathodoluminescence (CL) detector in a scanning electron microscope (SEM) to provide spectroscopic information along with image processing and visualization tools that enhances the quality and utility of that imagery. This system was initially tested using a ZnS standard known to produce a strong CL signal in the visible spectrum. Enhanced images and spectroscopic data could also be used for grain and spot targeting of natural zircons that commonly precedes isotopic analysis by laser ablation or ion microprobe. The filter-wheel system was made from inexpensive or 3D printed materials, allows for interchangeable filters for a variety of applications, and the switching between those filters without the user breaking SEM vacuum. The color filtered images were used to create color composite images similar to those generated by higher-end spectrometers with built-in color filtering capability. The embedded data from the RGB pixels of the color filtered images were then used to generate 2D and 3D graphs providing another visual path for comparing relative intensities. A color composite image and associated 3D graphs for a prototypical zircon sample was generated to demonstrate the usefulness of the device and utility of plots. Design documents and specifications for the color filter wheel, and codes to generate images and plots are available on https://weber.edu/cos/instrument_information.html.

https://doi.org/10.5194/egusphere-2022-83
Preprint. Discussion started: 22 June 2022

1 Introduction

Cathodoluminescence (CL), the emission of light resulting from bombardment of a material by an electron beam, can yield a variety of information about a material and hence is an important characterization technique. When observed from a sample in a Scanning Electron Microscope (SEM), the technique can yield both microscopic information (because of the microscopic focus of the electron beam) and spectroscopic information (because of the potential for spectroscopic analysis of the light *in situ*). The technique is widely used to provide information about semiconductors, phosphors, ceramics, electronic devices, and minerals (Yacobi and Holt, 1990). CL mapping has become a standard technique for imaging a variety of minerals. Examples include: imaging zircon in order to identify zonation/growth zones for geochronologic analysis (Hanchar and Miller, 1993); characterization of quartz microtextures, hydrothermal growth patterns, and sandstone detrital provenance signatures (e.g. review by Götze et al., 2001); and characterization of detrital, diagenetic, hydrothermal, and deformational components and porosity evolution in carbonate rocks (see overview by Hiatt and Pufahl, 2014).

In practice, there are technical difficulties associated with collecting and analyzing the CL spectrum from a sample within the vacuum chamber of an SEM. The light is typically emitted isotropically from the sample, but the collection apparatus cannot surround the sample without blocking the electron beam. The variety of detectors typically present in the SEM chamber for imaging with backscattered and secondary electrons create a crowded environment. Hence, CL detectors must be designed to fit in the complex environment of the SEM chamber. Although several commercial devices are available, cost may be a factor, especially if the technique is being used in a teaching or training environment, or if CL is not the primary imaging technique. Possible light collection methods include using reflective optics, refractive optics, fiber optics and/or light pipes (Coenen and Haegal, 2017). However, these techniques require precision alignment (Coenen et al, 2015) which is not always achievable.

https://doi.org/10.5194/egusphere-2022-83
Preprint. Discussion started: 22 June 2022

Previously reported home-built systems are quite complex (Beauvineau and Semo, 1982; Benitez et al., 2018). A less expensive option for adding CL capability to an SEM is the use of a broadband light detector (typically a silicon photodiode) that can easily be brought into close proximity of the sample curing electron-beam excitation, however this does come with a corresponding loss spectroscopic information. We present a home-built filter wheel apparatus that can be attached to a broadband detector to recover that lost information and therefore overcome the primary drawback of this less expensive option. The filter wheel itself is constructed by 3D printing and the control electronics can be assembled in a typical undergraduate electronics laboratory. We demonstrate the applicability of our device first with a study of ZnS where we show agreement with previous microscopic and spectroscopic CL studies (see section 7.3 of Yacobi and Holt, 1990) and additional use of the CL system to characterize internal zonation of zircons, which later underwent isotopic analysis, highlighting the techniques applicability to a common CL application in geochronology.

2 Materials and Methods

2.1 Color Filter Wheel and Mounting Cylinder Construction and Installation

The filter can be deconstructed to three main elements: color filter lenses, 3D printed parts for mechanical designs, and electronic parts supporting user input and motor control. The assembled filter exchange device is mounted on the CL detector in the SEM (Figure 1A) with the wheel holding the various filters (Figure 1B). Inexpensive plastic color filtering lenses can be purchased from a variety of sources. We analyzed each color filter using a Cary 60 ultra-violet visible (UV-VIS) spectrometer. Our design (Figure 1B) allows switching between four different filters and panchromatic imaging without breaking vacuum.

Due to the size and shape constraints inside the SEM, parts were designed using the CAD software, Autodesk Inventor, and subsequently 3D printed (all design documents and specifications can be found on our publicly available webpage https://weber.edu/cos/instrument_information.html). ABS plastic (a thermoplastic polymer) was used to ensure that the 3D printer parts would not affect the

https://doi.org/10.5194/egusphere-2022-83
Preprint. Discussion started: 22 June 2022

vacuum within the SEM by off gassing. The surfaces of the parts were sealed using acetone to further prevent off gassing.

The 3D printed pieces include: the rotating "wheel" (sector of a circle, Figure 1B) to hold the filters, the suspension basket to hold the servo motor needed for precision positioning (Figure 1A) and the aforementioned wheel, a mounting cylinder to secure the basket to the CL detector (Figure 1A). The wheel also has a mounting hole to secure itself to the drive shaft of a servo motor. The suspension basket holds the servo motor and filter wheel and is custom fit to the specific servo chosen for our design. The mounting cylinder was designed to hold the basket at the appropriate height beneath the CL detector in order to align the filters in front of the detector. The mounting cylinder has a simple design that allows it to slide over the CL detector. A box was designed to encase the printed circuit board assembly that is used to control the servo motor external to the SEM chamber. The user interface (Figure 2) was designed to allow filter selection and rotation without breaking vacuum and is external to the SEM chamber. The desired filter can be selected or changed using a keypad (Figure 2).

The wheel has six posts creating five windows, or slots to hold the filters. The center window remains empty for an initial panchromatic image. Filter positions are programmed to positions 1 through 5, which the user presses. Once selected, the servo motor rotates the selected filter into place. The servo motor was designed to rotate 180 degrees and controlled with a Pulse Width Modulation (PWM) signal. With the filters arranged around the circular edge of the filter wheel, the servo motor rotates to the exact degree necessary to place the selected filter in front of the lens.

Wires are connected to both sides of an unused feedthrough port on the SEM to wire power and the PWM signal to the motor. The last feature, the display informing the user of the current filter selection, was completed by using a 20 x 4 liquid crystal display.

These three devices were connected using an Atmega 328P-PU microcontroller. The chip was programmed using the Arduino IDE due to the extensive amounts of available libraries. Finally, all applicable parts were soldered to a custom designed PCB made using Circuit Maker software and printed by Oshpark.

2.2 Testing of Color Filter Wheel Functionality

https://doi.org/10.5194/egusphere-2022-83
Preprint. Discussion started: 22 June 2022

In order to test the color filter wheel apparatus we used a common mineral standard, ZnS, to compare sample emissions peaks which those in the published literature (e.g. Yakobi and Holt, 1990). Wavelengths for each color filter, blue, green, red, and yellow, were estimated using data above a 20% transmittance threshold. After obtaining an image without a filter (Figure 3E), we rotated through the colored filters. The contrasts and brightness were adjusted for the initial panchromatic image (Figure 3E) but were not adjusted in between the filters (Figure 3A-D) in order to maintain the image characteristics.

3 Results

3.1 Filter Wheel Validation using ZnS Standard

CL images of a ZnS standard sample with strong luminescence in the visible portion of the spectrum (Figure 3A-D) and the transmittance curves for the filters (Figure 3F) were obtained from a Cary 60 ultraviolet/visible spectrometer. A qualitative comparison of these images shows the blue image (Figure 3A) is brightest and therefore more of the luminescence for the ZnS penetrates the blue filter compared to the others. Hence, the sample emission must have a relative peak in this range in accordance with other studies (see section 7.3 of Yacobi and Holt, 1990). Despite significant overlap in transmittance for the green and blue filters, the blue image is significantly brighter (Figures 3A and 3B). This discrepancy between images allows us to narrow our peak suggesting there is a peak in the 390 nm – 420 nm range where the blue filter is transmitting well but the green is not. It is important to note that relative intensity is significant rather than absolute intensity. Summing the intensities of the filtered images does not necessarily result in the absolute intensity of the panchromatic image. Given the overlap in the transmission wavelengths of the filters, photons may be double counted between images or photons may be missed by the particular color filters chosen.

4 Application of Color Filter Wheel in Imaging Zircon

The mineral zircon ($ZrSiO_4$) is widely used to decipher the histories and origins of igneous, metamorphic and sedimentary rocks. Zircon incorporates relatively high concentrations of radioactive

https://doi.org/10.5194/egusphere-2022-83
Preprint. Discussion started: 22 June 2022

uranium (U) and thorium (Th) during crystal growth, is present in many rocks, has a high closure temperature for the U-Th-Pb (lead) dating system (depending on radiation damage), is chemically and physically resistant to breakdown, and therefore is the most commonly analyzed accessory mineral for U–Th–Pb geochronology. Due to its resistant nature, many zircon grains contain multiple growth zones related to phases of magmatic crystallization, metamorphism, alteration, and recrystallization (Hanchar and Miller, 1993). These growth zones and internal structure can be revealed by detailed CL imaging of grains, which is a common and necessary step preceding isotopic analysis.

The filter wheel system also allows for the creation of color composite images similar to what can be generated using a color CL system, which were used to help target various crystallographic domains for isotopic and elemental analysis. The composite image helps highlight that the zonation within and between zircon crystals that can originate from various luminescent mechanisms. Blue CL is associated with electron vacancies from SiO_4 groups, yellow CL is associated with radiation damage, and red CL is associated with the incorporation of trace elements, specifically Dy (Götze, 2012). The distinct contrast between the background and the zircon grain in the BSE image (Figure 4A) is used to reduce the noise of the initial CL image (Figure 4B) (Michels pers. com. January 26, 2022). Any pixel in the BSE image below an intensity threshold chosen from the dark region, is then discarded in the CL image to produce the crisp CL image (Figure 4C). This noise reduction technique is used in all the CL images, both panchromatic and filtered (Figure 4D). Using the pixel data from the filtered images, grayscale images or composite images were created from the filtered data and then 2D or 3D plots of the intensity data from each filtered image were generated (Figure 5) providing a new visualization pathway for viewing the data obtained from the filter wheel.

Image division was also used to further explore changes in relative intensity between the color filtered images by dividing the pixel data from each image. Figure 6 shows the division between the red filtered image and blue, green, and yellow filters, respectively, for the line of pixels (red) shown in the inset panchromatic CL image. The black vertical lines show the locations in each graph where the red filter has a higher relative intensity than the surrounding areas. The pixel location, denoted by the red circle, has the highest relative red intensity and corresponds to a very small grain shown by the circle in the CL image. This technique seems particularly useful for applications with large mineral mounts

https://doi.org/10.5194/egusphere-2022-83
Preprint. Discussion started: 22 June 2022

and/or thin section mapping where the user is trying to find features that are difficult to see on the SEM. All image processing and analysis were completed in Python and are available by request.

5 Conclusions

Our results show that these inexpensive filters allow for semi-quantitative analysis, which could be improved with the purchase of higher quality filters with less transmission overlap. This filter wheel system can greatly expand the capabilities of a broadband CL detector. The overall design of the filter wheel can be adjusted as necessary to accommodate different chamber configurations and specifications. In an educational or training environment, this inexpensive system provides an avenue for learning new techniques in image processing and data science (Rector et al., 2017) and also provide a platform for a discussion into filter efficiency and their impacts on data collection. Our image processing techniques also generated images which allowed us to identify multiple domains within complicated zircons to target for isotopic analysis. We plan to explore the use of 2D and 3D plots along with the image division techniques to assist with targeting in single mineral mounts and thin section mapping in the future.

Code/Date Availability

Design documents and specifications for the color filter wheel, and codes to generate images and plots are available on https://weber.edu/cos/instrument_information.html.

Author Contributions

K. Rabosky was the main supervisor providing project conceptualization, troubleshooting with design, construction, instillation, and use of the filter wheel, led image processing and data analysis, and was lead author on the manuscript. C. Inglefield provided additional supervision to the overall instrument design, utilization, and support writing the manuscript. E. Balgord provided the geologic supervision and project conceptualization with the addition of zircon image analysis, and work on writing the manuscript. S. Stamps and C. Jones contributed to the SEM imaging, validation, and analysis

https://doi.org/10.5194/egusphere-2022-83
Preprint. Discussion started: 22 June 2022

of the project. S. Stamps wrote the original draft of sections 2.2 and 3.1. C. Jones also contributed to the python code used in this project. B. Lee and M. Totland designed and built the filter wheel instrument in this paper, the main resource for this project and wrote the initial draft of Section 2.1 of this paper. J. Mathews designed and built an initial filter wheel instrument that was used as the foundations for the second-generation instrument outlined in this paper.

Acknowledgements

Funding for this project was provided through grants from Weber State University (WSU) Research, Scholarship and Professional Growth to K. Rabosky and E. Balgord. Zircon separations were completed at Weber State University, Idaho State University and Zirchron LLC. Conversations with faculty and staff from the University of Arizona Laserchron Center (supported by NSF-EAR 1649254), specifically Zachary Michels, provided key insight into handling the CL background for these images. Leigh Komperda, the technician for the College of Science at WSU, also provided help with maintaining our SEM and creating the repository of documents for this publication.

References

Beauvineau, J. and Semo: Improved spectrometer for cathodoluminescence studies in scanning electron microscopy, J. Rev. Sci. Instrum., 53(10), 1573-1576, doi: 10.1063/1.1136838, 1982.

Benitez, A., Santiago, U., Sanchez, J., and Ponce, A.: Design of a cathodoluminescence image generator using a Raspberry Pi coupled to a scanning electron microscope, Rev. Sci. Instrum. 89, 013702, doi: 10.1063/1.4986044, 2018.

Coenen, T. and Haegel, N.: Cathodoluminescence for the 21st century: Learning more from light. Applied Physics Reviews, 4, 031103, doi: 10.1063/1.4985767, 2017.

Coenen, T., Brenny, B. Vesseur, E. and Polman, A.: Cathodoluminescence microscopy: Optical imaging and spectroscopy with deep-subwavelength resolution, MRS Bulletin, 40, 359-365, doi: 10.1557/mrs.2015.64, 2015.

Götze, J.: Application of Cathodoluminescence Microscopy and Spectroscopy in Geosciences, Microsc. Microanal., 18, 1270-1284, doi: 0.1017/S1431927612001122, 2012

https://doi.org/10.5194/egusphere-2022-83
Preprint. Discussion started: 22 June 2022

Götze, J., Plötze, M. and Habermann, D.: Origin, spectral characteristics and practical applications of the cathodoluminescence (CL) of quartz–a review, Mineralogy and Petrology, 71, 3, 225-250, 2001.

Hanchar, J.M., Miller, C.F.: Zircon zonation patterns as revealed by cathodoluminescence and backscattered electron images: implications for interpretation of complex crustal histories. Chem. Geol. 110, 1–13, 1993

Hiatt, E.E. and Pufahl, P.K., 2014, Cathodoluminescence petrography of carbonate rocks: a review of applications for understanding diagenesis, reservoir quality, and pore system evolution: Mineralogical Association of Canada Short Course 45, p. 75-96. Fredericton NB, 2014

Michels, Z., January 2022, University of Arizona, LaserChron Lab, personal communication.

Rector, T., Levay, Z., Frattare, L., Arcand, K., and Watzke, M.: The Aesthetics of Astrophysics: How to make appealing color-composite images that convey science, PASP, 129, 058007, doi: 10.1088/1538-3873/aa5457, 2017.

Yacobi, B., and Holt, D.: Cathodoluminescence Microscopy of Inorganic Solids, New York: Plenum Press, 1990.

https://doi.org/10.5194/egusphere-2022-83
Preprint. Discussion started: 22 June 2022

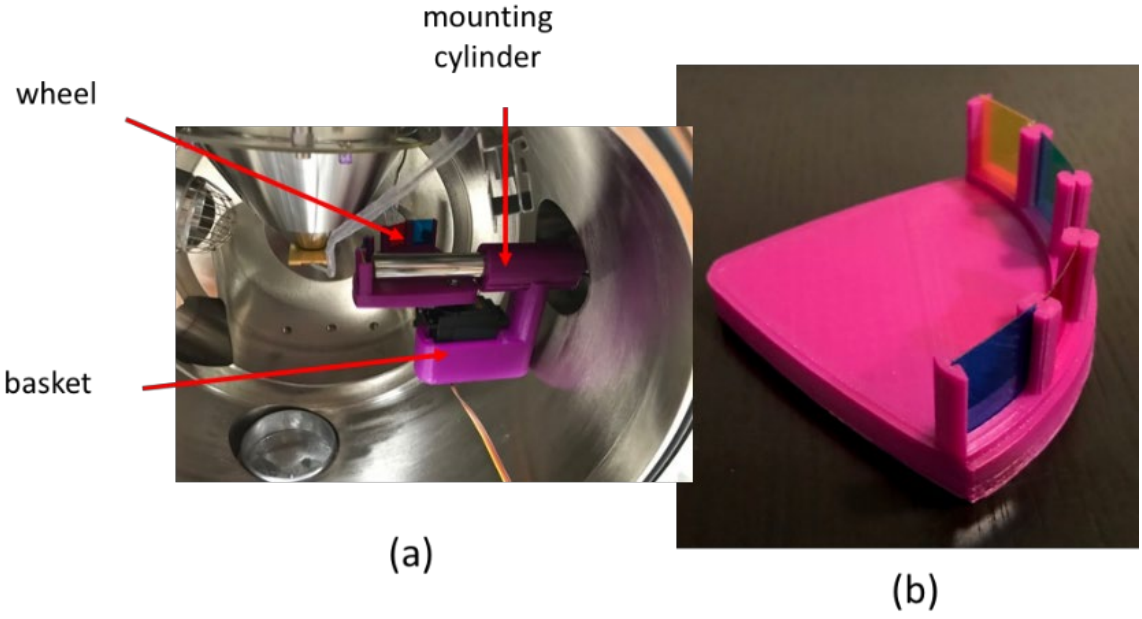

234
235
236 Figure 1: A. Picture taken inside of the vacuum chamber of the SEM showing the filter wheel exchange
237 device fully assembled and mounted on the cathodoluminescence detector. B. The spinning wheel
238 mount apparatus holding the four exchangeable color filters. Note, the center is left open to compare
239 the total amount of light transmitted without a filter to the amount transmitted through the various color
240 filters.

241

https://doi.org/10.5194/egusphere-2022-83
Preprint. Discussion started: 22 June 2022

Figure 2: User interface with output LCD screen and input keypad used to drive the motion of the filter exchange device.

https://doi.org/10.5194/egusphere-2022-83
Preprint. Discussion started: 22 June 2022

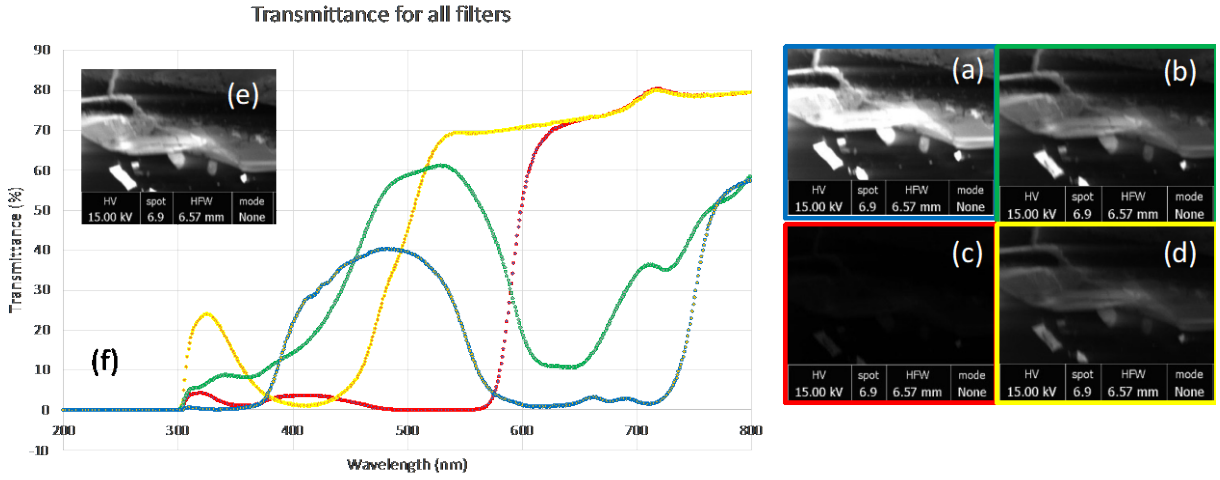

Figure 3: ZnS CL images using (a) blue filter (b) green filter (c) red filter (d) yellow filter (e) no filter (f) Transmission data for color filter used to image (a) – (d).

https://doi.org/10.5194/egusphere-2022-83
Preprint. Discussion started: 22 June 2022

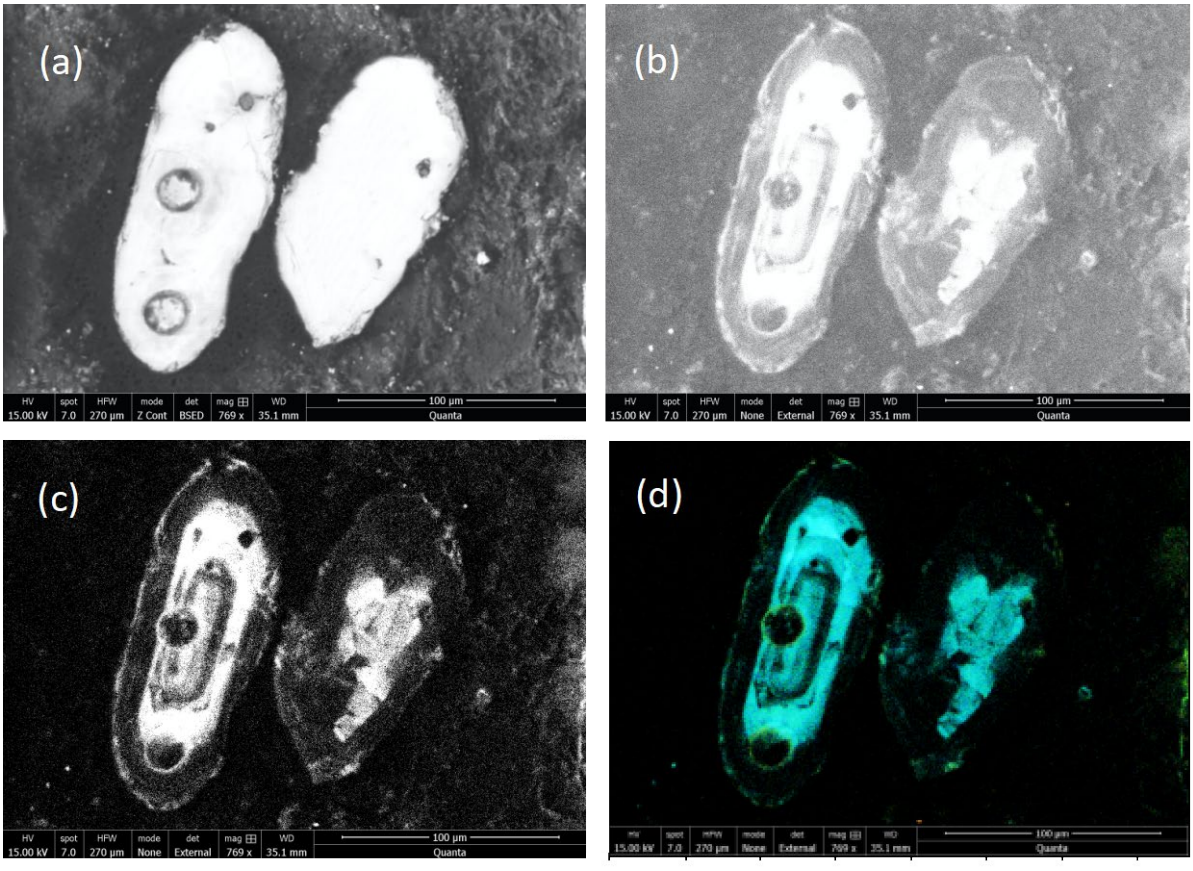

Figure 4: A. BSE image of two zircon crystals within a mount; B. CL without background subtraction; C. Panchromatic CL image of the same zircon crystals with background subtraction; and D. Final color composite image also with background subtraction.

https://doi.org/10.5194/egusphere-2022-83
Preprint. Discussion started: 22 June 2022

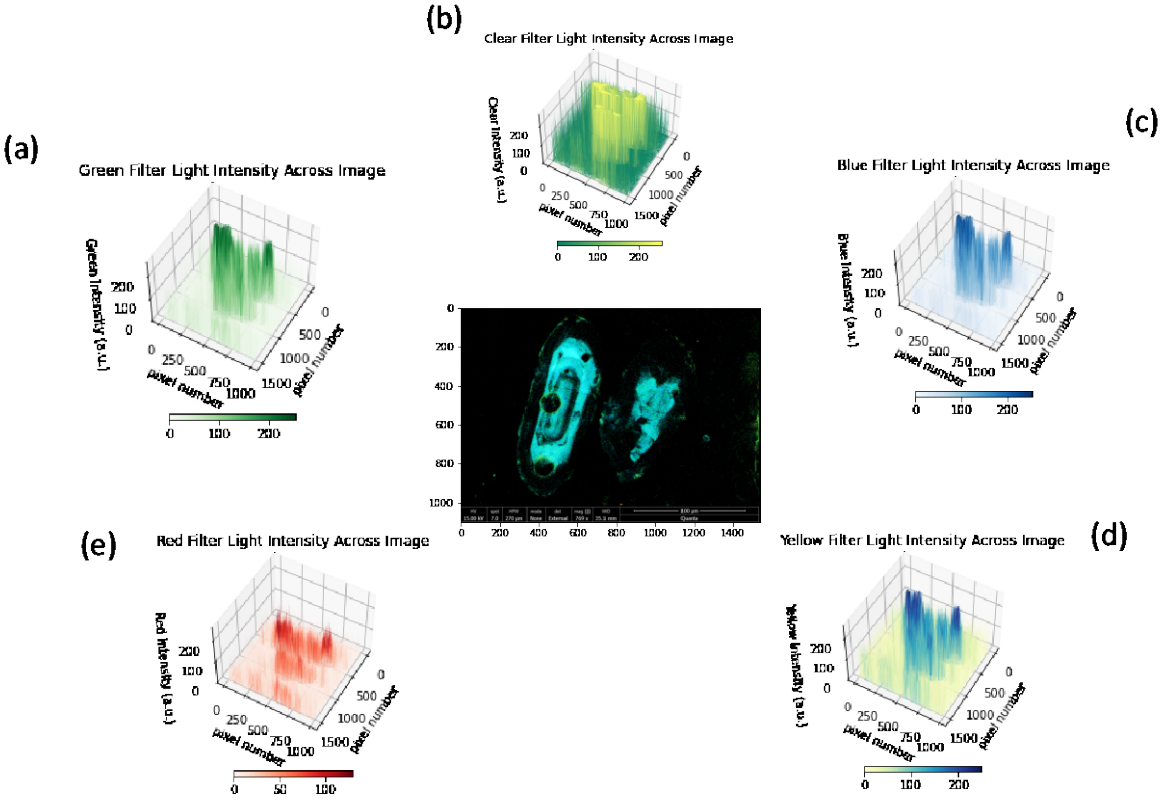

Figure 5: Center: RBG composite image of zircon crystal. (a)-(e) are 3D graphs of the intensity data from the green, clear, blue, yellow and red filters respectively.

https://doi.org/10.5194/egusphere-2022-83
Preprint. Discussion started: 22 June 2022

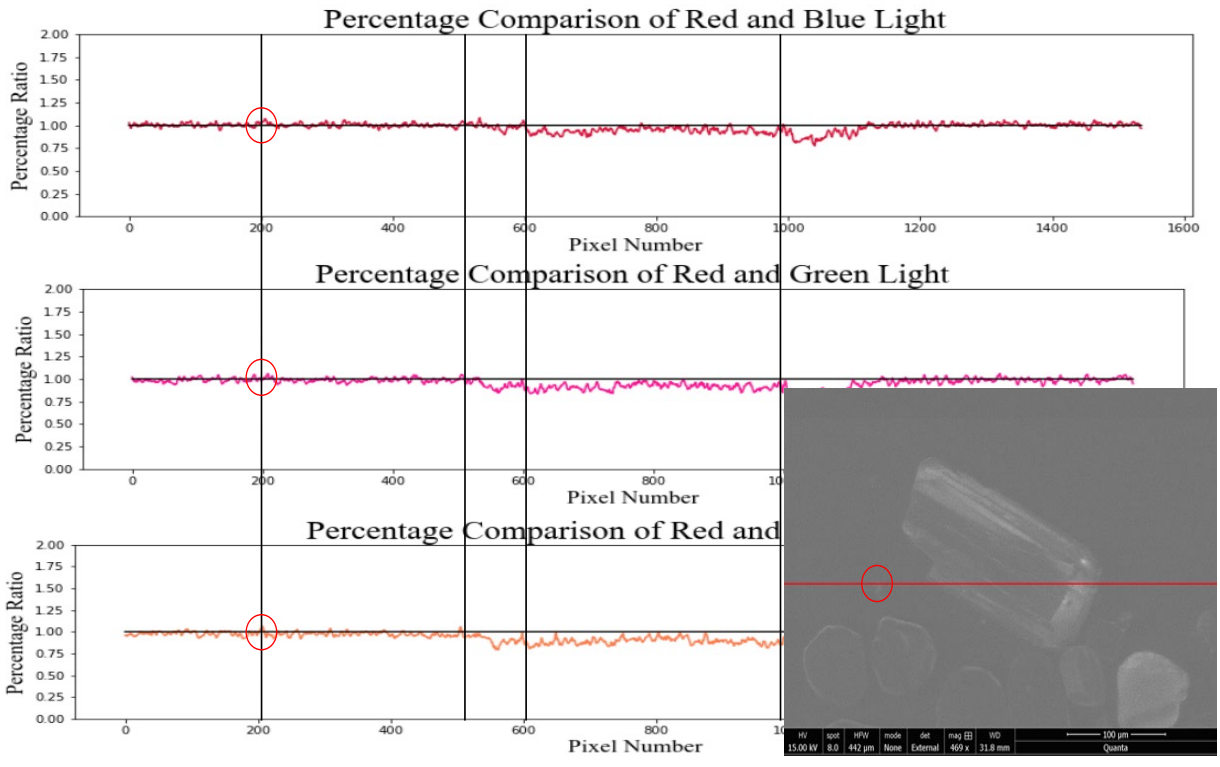

Figure 6: Color filter image division for one row of pixels shown by red line in CL inset image (top) red divided by blue (middle) red divided by green (bottom) red divided by yellow.